J Mater Sci (2022) 57:15464–15473

Energy materials

Preparation of Fe-dispersed porous carbons from iron alum/carboxymethylcellulose gels and their application to volatile organic compound adsorption

Naoya Miyajima[1,*], Kazuo Hara[2], Hideto Sakane[1], and Kazusada Suzaki[3]

[1] *Graduate Faculty of Interdisciplinary Research, University of Yamanashi, 4-4-37 Takeda, Kofu, Yamanashi 400-8510, Japan*
[2] *Interdisciplinary Graduate School of Medicine and Engineering, University of Yamanashi, 4-4-37 Takeda, Kofu, Yamanashi 400-8510, Japan*
[3] *Cement Business Division, DC Co., Ltd., 1-1 Asano-cho, Kawasaki-ku, Kawasaki, Kanagawa 210-0854, Japan*

Received: 1 March 2022
Accepted: 22 July 2022
Published online: 4 August 2022

ABSTRACT

The simple preparation of porous carbons with highly-dispersed metal particles and no additional activation by gelating iron alum and carboxymethylcellulose sodium (CMC-Na) was investigated. Various porous carbons with different pore structures were prepared by varying the mass ratio of iron alum to CMC-Na. In carbonizing the gels, Na_2CO_3 by-product acted as an activator and promoted pores formation by decomposing over 700 °C. Carbonization of the CMC-Na xerogels with more Fe content resulted in the formation of α-iron (iron(*cI*2)) nanocrystals in porous carbons. Because the carbons exhibited typical ferromagnetic behavior, they could be collected by a neodymium magnet in water. The porous carbons which include other sodium compounds that improved adoption for volatile organic compound (VOC) demonstrated good VOC removal abilities compared to a commercial activated carbon. Their developed pores would facilitate accessing of VOC adsorbates to the carbon.

Handling Editor: Andrea de Camargo.

Address correspondence to E-mail: miyajima@yamanashi.ac.jp

https://doi.org/10.1007/s10853-022-07578-x

GRAPHICAL ABSTRACT

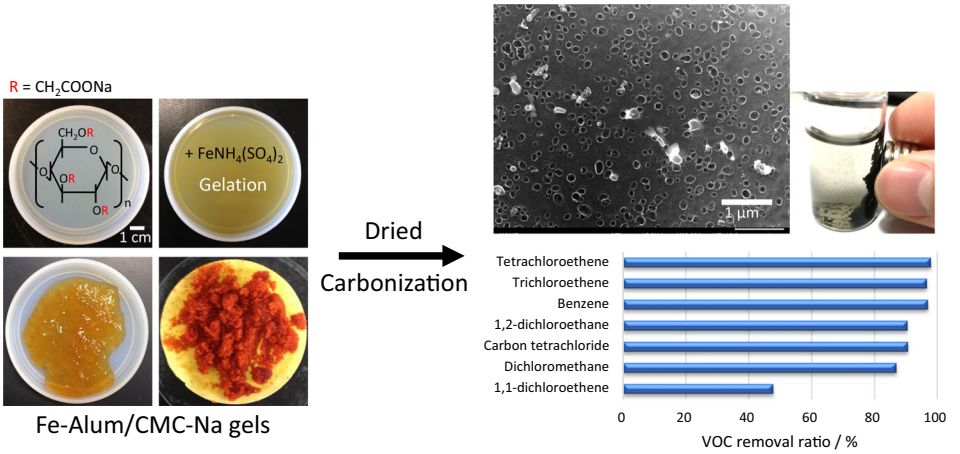

Introduction

Porous carbons, e.g., activated carbon, have well-developed pore structures and are widely used for adsorption and separation. To improve the adsorption properties, it is necessary not only to control the pore structures of carbon more precisely but also to combine carbon with various species such as heteroatoms, metals, and metal compounds [1, 2]. The combinations with metal species can easily improve adsorptivity by carbon surface modification. Typical combining methods are dispersion and doping of metal species in the carbon matrix and provide some unique properties depending on metal or metal oxide additives [3–8]. The loading metal species can also change the type and amount of surface functional groups on carbon, which has a positive effect on various adsorption properties [4, 6]. Meanwhile, the combinations were fraught with practical issues such as cost, synthesis process, and environmental problem.

Carbonizing a mixture of metal compound and polymer is a simple and rather inexpensive method for dispersing the metal in carbon [9–13]. Recently, pyrolysis of metal-containing organic precursors has been extensively studied to functionalize the carbons with porous coordination polymer (POP) or metal–organic framework (MOF) which is received a lot of attention for highly simultaneously controlling metal dispersion and pore structures [14–18]. Carbonizing POP or MOF in an inert atmosphere gives a highly dispersed metal nanoparticles encapsulated with a porous carbon matrix. A high surface area is generally achieved by removing out these metal particles or by pyrolysis of the MOF precursor [18]. Metal/carbon hybrids can be produced by controlling the type of MOF and the carbonization temperature, imparting the catalytic properties of MOF-derived metal species.

Carboxymethylcellulose (CMC) is a polysaccharide consisting of glucose units modified with cation-exchangeable carboxymethyl groups. CMC and Na^+-exchanged CMC, CMC-Na, are non-toxic and inexpensive and are widely used in foods and medicines. CMC disperses more easily in water than cellulose when it is exchanged to CMC-Na. The degree of substitution (DS) for the carboxymethyl group (etherification) and the average molecular weight (AMW) of CMC affect its solubility and viscosity of CMC-Na solution, respectively [19]. CMC-Na aqueous solution easily gels with metal salts of multivalent metal ions because the carboxymethyl groups can be cross-linked by the metal ions. As a result, alum is often used as a food additive to adjust the

viscosity of CMC-Na gels in the industrial setting [20, 21]. Such CMC-Na gels are promising precursors to provide metal-dispersed carbon. Carbonization over 800 °C of CMC-Na was introduced lots of pore to carbon by chemical activation of Na_2CO_3 by-products [22]. Simple carbonization of CMC-Na gel exchanged for some proper metal ions may induce a metal-loaded porous carbon without additional activation and will provide useful information for a new metal/carbon composite design.

CMC-Na gels with iron alum that is one of the common alums were prepared and carbonized to synthesize Fe-dispersed porous carbons that will be magnetic adsorbents. The pore and the magnetic properties of the obtained carbons were studied and the environmental purification property was demonstrated by volatile organic compounds (VOC) adsorption.

Materials and methods

Sample preparation

Commercially available carboxymethylcellulose sodium powder (CMC-Na, DS = 0.7, AMW = 250,000, Acros Organics, Co.) was gradually added to 100 mL aqueous solution of iron alum (FeA, $FeNH_4(SO_4)_2$•$12H_2O$, Kanto Chemical, Co, Inc.) for gelation. The mass ratio of FeA/CMC-Na in solution was adjusted to 0, 0.05, 0.15, or 1.0. Each gel was dried at 60 °C for 24 h and will be denoted as CFeAx (x = 0, 0.05, 0.15, or 1.0). Prepared xerogels were carbonized at 700 °C or 900 °C for 1 h under high-purity nitrogen flow and will be denoted as cy-CFeAx (y = 700 or 900). The carbonization yield was calculated using the mass ratio of the carbonized sample to the starting xerogel.

Characterization

The thermal behavior of the xerogels during carbonization was investigated by TG–DTA (TG-DTA2000S, MacScience) under argon flow. X-Ray diffraction (RINT-Ultima$^+$, Rigaku) and nitrogen gas adsorption at 77 K using a volumetric apparatus (BELSORP-mini, MicrotracBEL) were examined for the crystalline structure and the porosity of the carbons, respectively. The specimens for adsorption were preheated at 300 °C in argon flow. The total pore volume (V_{tot}) and the micropore surface area (A_{micro}) were calculated from the nitrogen adsorption isotherms using α_s method [23]. The morphology and the dispersion of metal species in the carbons were studied by FE-SEM–EDX (JSM-6500F, JEOL). Atomic absorption spectroscopy (Z-6100, Hitachi) was used to investigate the contents of Fe and Na in carbon. The carbons were burned off under air atmosphere and their residual ash was dissolved in hydrochloric acid for the analysis of metal contents.

Magnetization (M) of the carbons was measured with a physical property measurement system (PPMS, Quantum Design) at a temperature of 5 K, 100 K, and 300 K in magnetic fields ranging from 0 to 1 T. The zero field cooled magnetization (M_{ZFC}) and the field cooled one (M_{FC}) for c700-CFeA1.0 were also measured at a temperature from 5 to 300 K in constant magnetic fields of $\mu_0 H$ = 0.01, 0.1, 1, and 3 T. M_{ZFC} was measured with increasing temperature at first and M_{FC} was measured with decreasing successively.

The VOC adsorption test was performed under JIS K 0125. The carbons of 0.1 g were added 700 ppb of thirteen kinds of VOCs standard solution of 10 mL and were stirred for 4 h. The solutions were filtered and analyzed by GC–MS (JSM-Q1050GC, JEOL). The GC separation was carried out on a capillary column (Inert Cap AQUATIC; 0.32 mm i.d. × 60 m, film thickness 1.40 μm, GL science Inc.). The blank of chromatograms was corrected by measuring each with VOC component without the carbons. The quantitative analysis of Cl^- produced by the decomposition of some of the VOCs was performed using the same apparatus.

Results and discussions

Characterization of Fe-loaded porous carbon

Hydrogel was formed from CFeAx with $x \leq 0.15$ but solid precipitate was formed at x = 1.0 because of the insolubility of higher cross-linking density in the polymer [20] (Fig. S1). The reference [20] stated that when the value of x exceeded 0.2, solid precipitation insoluble in water formed, which was confirmed in our preparation too. Each hydrogel was converted to its respective xerogel by drying at 40 °C overnight.

Figure 1 shows TG–DTA curves of CFeAx. All samples exhibit gradual weight loss until around

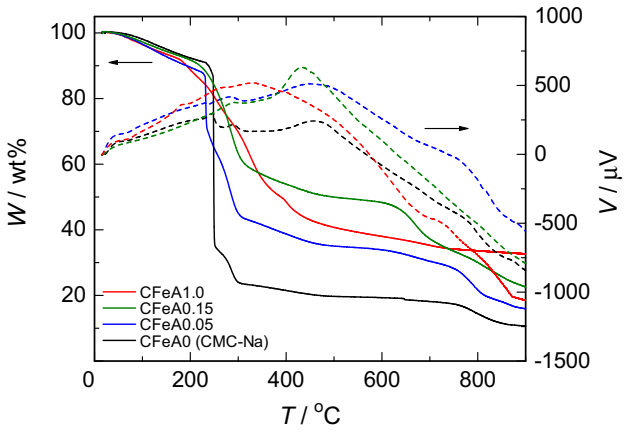

Figure 1 TG–DTA curves of CFeA*x*. Solid and broken lines indicate TG and DTA curves, respectively.

250 °C and then remarkable weight loss due to the decomposition of the carboxylmethylglucose unit of CMC. This weight loss decreases as x increases and an additional weight loss is shown again over 700 °C except CFeA1.0. These losses indicated the oxidation by $2C + Na_2CO_3 \rightarrow 3CO + 2Na$ reaction with a carbon loss [22, 24]. The lack of activation in CFeA1.0 suggests that the most of Na^+ were exchanged for Fe^{3+} in the gels and negligible Na_2CO_3 was created.

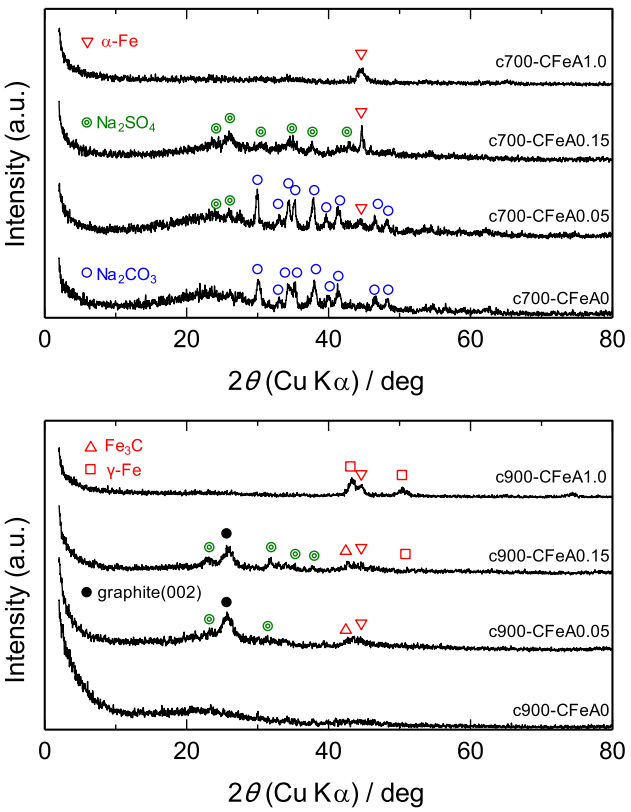

Figure 2 XRD patterns of c*y*-CFeA*x*.

Figure 2 shows XRD patterns of the carbonized samples. The XRD pattern of c700-CFeA0.05 is similar to that of c700-CFeA0, in which the peaks assigned to Na_2CO_3 were superimposed onto the broad pattern of nongraphitic carbon. The peaks assigned to α-iron (iron(*cI*2)) become clearer with increasing x. The peaks assigned to Na_2CO_3 are disappeared by carbonization at 900 °C, supporting the interpretation from Fig. 1 of the Na_2CO_3 decomposition over 700 °C. The patterns for c900-CFeA0.05 and c900-CFeA0.15 show peaks assigned to Fe_3C and rather sharp graphite(002) at around 26°. They proposed that graphitic carbon components were produced via Fe_3C which was reported as catalytic graphitization phenomenon by iron [25]. c900-CFeA1.0 represents the peaks assigned to γ-iron (iron(*cF*4)), implying that some γ-iron particle, the stable phase at above 906 °C, was remained in carbon by the rapid quenching. Scherrer's equation estimated the crystallite diameter of α-iron (iron(*cI*2)) in c900-CFeA1.0 was approximately 7 nm.

Table 1 shows carbonization yield and Fe and Na contents of the carbonized samples. All of the yields of carbonized at 700 °C are about 35 wt%, whereas those at 900 °C decrease with decreasing x in accord with their TG changes in Fig. 1. The Fe contents in carbons increase with increasing x. On the contrary, the Na content in c900-CFeAx significantly decreases probably because of the decomposition of Na_2CO_3 or the vaporization of other sodium species. The least Na contents in cy-CFeA1.0 indicate that Na^+ eluted by exchange for Fe^{3+} during the gel preparation.

FE-SEM images of some carbonized samples are shown in Fig. 3. Arrows in Fig. 3a point out that carbon particles of c.a. 10 μm in diameter were surrounded with needle-like crystals pointed out in Fig. 3b for c700-CFeA0.15. The carbon surfaces have numerous holes like a crater with nanometer-order openings on the sample. Meanwhile, in c900-CFeA0.05 and c900-CFeA0.15 (Fig. 3 c–f), the smoother carbon particles have numerous holes with irregular-shaped small crystals rather than the needle-shaped ones, in which the number and the size of the irregular crystals seems to increase with increasing x (Fig. 3d, f). On the other hand, flake-like carbon particles with few holes are observed in c900-CFeA1.0 (Fig. 3g, h). EDX analysis of c900-CFeA0.15 shown in Fig. 4 suggests that these irregular-shaped

Table 1 Carbonization yield, Na and Fe contents, and pore parameters

Sample	Carbonization yield/wt%	Na content/wt%	Fe content/wt%	A_{micro}/(m^2/g)	V_{tot} / (mL/g)
c700-CFeA0	35.8	–	–	3	0.04
c700-CFeA0.05	35.7	13.2	1.1	5	0.03
c700-CFeA0.15	34.3	17.5	4.1	60	0.10
c700-CFeA1.0	34.8	1.7	20.8	440	0.14
c900-CFeA0	18.0	2.2	0	950	0.52
c900-CFeA0.05	20.3	5.3	2.6	440	0.50
c900-CFeA0.15	25.1	7.3	5.8	220	0.32
c900-CFeA1.0	33.1	1.2	20.9	310	0.13

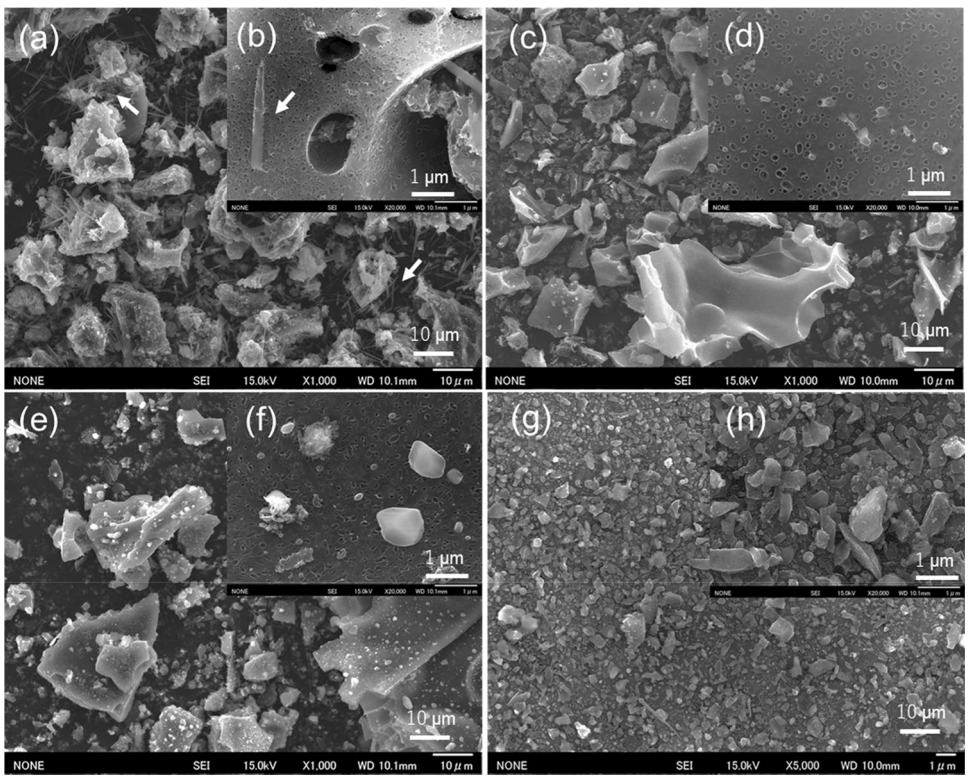

Figure 3 FE-SEM images of **a** and **b** c700-CFeA0.15, **c** and **d** c900-CFeA0.05, **e** and **f** c900-CFeA0.15, and **g** and **i** c900-CFeA1.0.

particles were Na_2SO_4. Fe species such as Fe_3C and metallic Fe diffused widely in c900-CFeA1.0 which had more Fe content (Fig. S3). These results suggest that the decomposition and disappearance of the needle-like crystals over 700 °C coincide with those for Na_2CO_3 diffraction line in Fig. 2 and introduced lots of holes in the carbon.

Figure 5 shows nitrogen adsorption isotherms at – 196 °C of *cy*-CFeA*x* and Table 1 summarizes their calculated pore parameters. c700-CFeA*x* except c700-CFaA1.0 indicate little adsorption whereas c900-CFeA*x* does significantly at $p/p_0 \approx 1$ with an adsorption/desorption hysteresis loop. It is indicated again that the Na_2CO_3 decomposition provided micropores and mesopores. These pore developments depended on Na content in the prepared xerogels. In other words, the lower the mass ratio of Fe is, the higher A_{micro} and V_{tot} become. In c700-CFeA1.0, the pores could also be developed by iron species activation or catalytic graphitization. It seems from the increments in nitrogen adsorption that Na species were more effective to develop micropores in carbon at these carbonization temperatures.

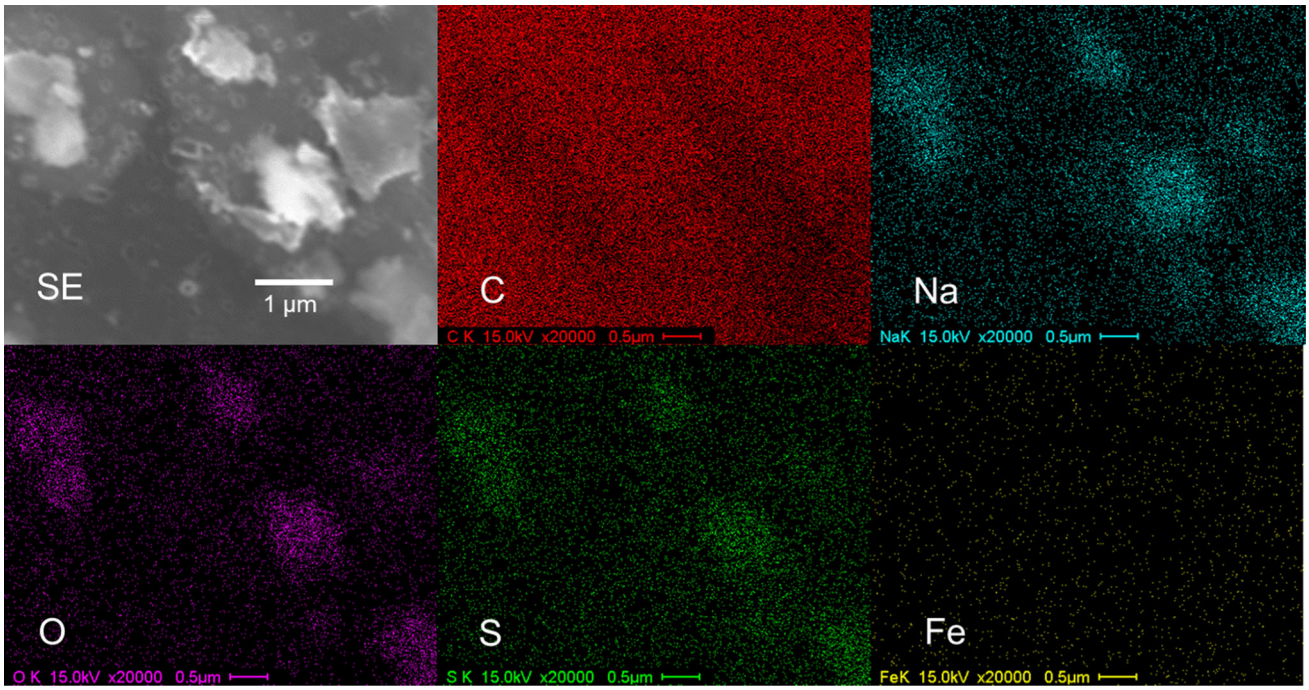

Figure 4 EDX mapping images of c900-CFeA0.15.

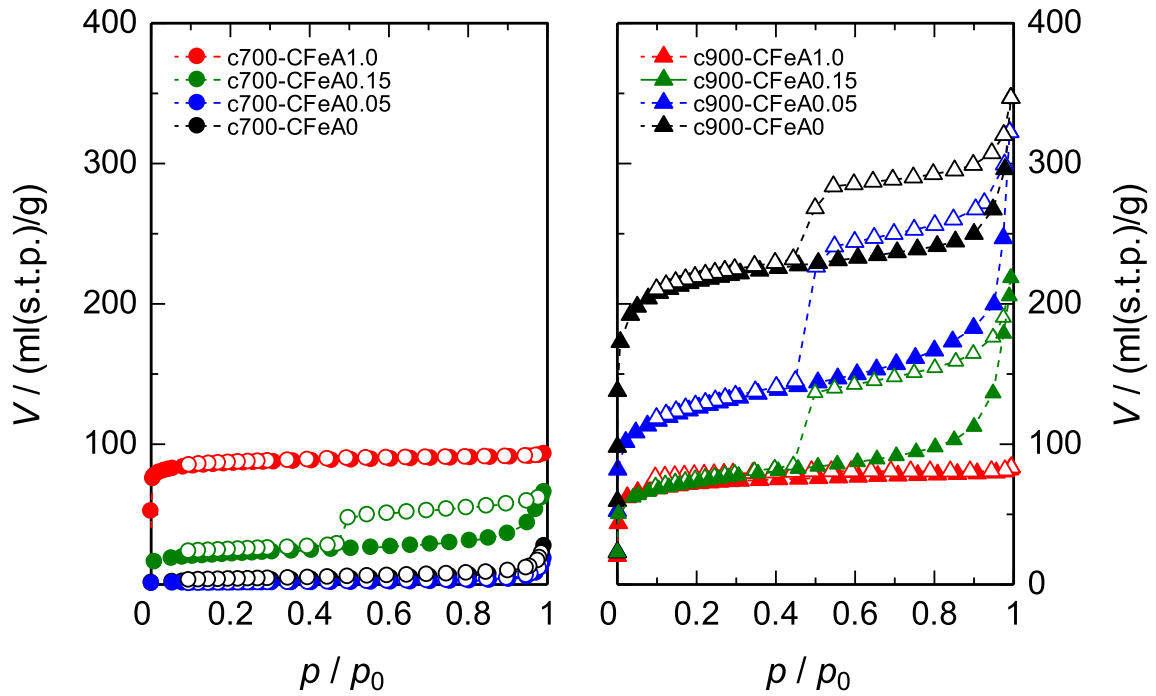

Figure 5 N_2 adsorption/desorption isotherms at –196 °C of c*y*-CFeA*x*.

Magnetization and VOC adsorption

Figure 6 shows magnetization curves for c900-CFeA*x*. c900-CFeA0 exhibits diamagnetism whereas c900-CFeA0.05 and c900-CFeA1.0 do ferromagnetism with a hysteresis loop. In the right panel, the area enclosed by the hysteresis loop for c900-CMC-FeA1.0 decreases with increasing the measurement temperature. These behaviors are typical of the aggregates of ferromagnetic fine particles and can be mainly caused

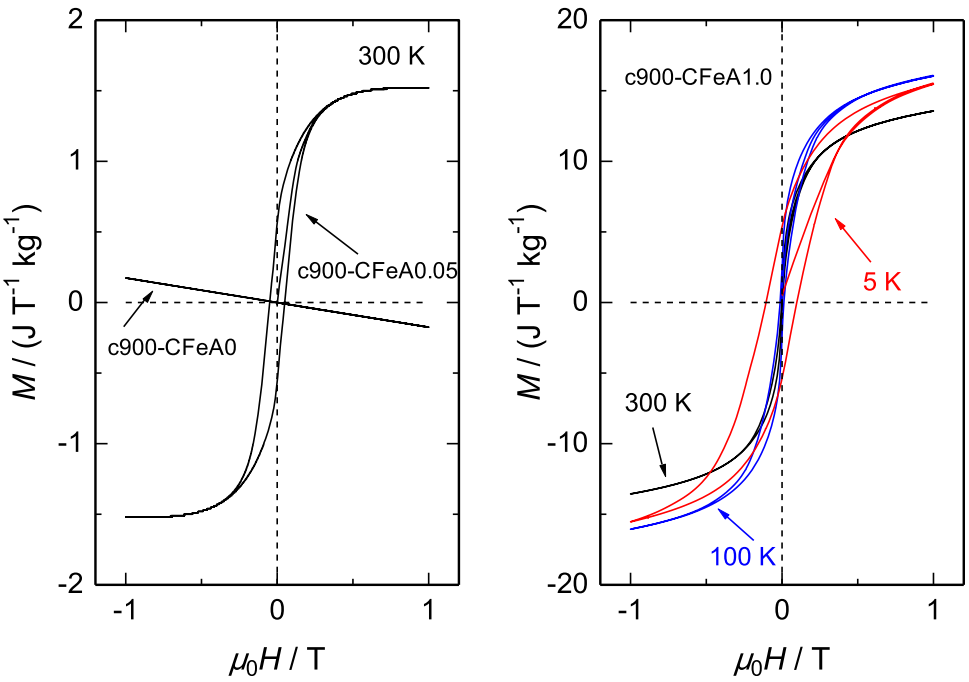

Figure 6 Magnetization curves for c900-CFeA*x*.

by α-iron components dispersed in the carbons [9, 13]. The saturation magnetization of c900-CFeA0.05 and c900-CFeA1.0 at 300 K was approximately 1.5 J T^{-1} kg^{-1} and 10 J T^{-1} kg^{-1}, respectively. Based on the saturation magnetization of α-iron at room temperature of 217.2 J T^{-1} kg^{-1}, the mass fractions of ferromagnetic components in both of the carbons were estimated to be about 0.69% and 4.6%, respectively, which corresponded to about 20% of Fe contents in Table 1. The whole dispersed particles of c*y*-CFeA*x* in water, except for c*y*-CFeA0 with diamagnetism, were attracted by a neodymium magnet, one of the rare earth permanent magnets mainly composed of neodymium, iron, and boron, indicating the possibility of their magnetic separation (Fig. S2).

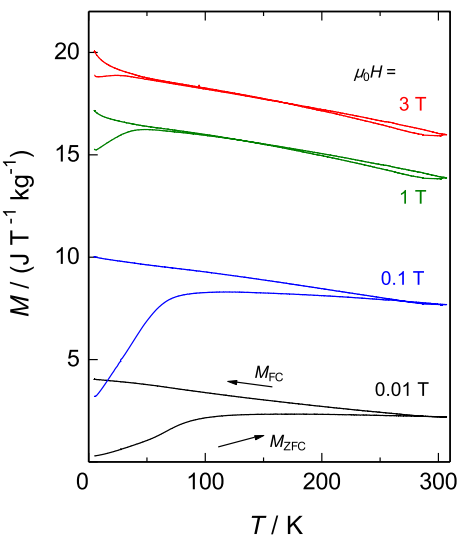

Figure 7 Temperature dependences of M_{ZFC} and M_{FC} under various constant magnetic fields for c900-CFeA1.0.

Figure 7 shows temperature dependencies of M_{ZFC} and M_{FC} in various constant magnetic fields for c900-CFeA1.0. Under the magnetic fields of 1 T and 3 T, M_{ZFC} exhibit a small hump around 45 K and converge with M_{FC} at the higher temperatures. M_{ZFC} decrease but M_{FC} increase with decreasing temperature below 45 K. The differences between M_{ZFC} and M_{FC} become more apparent at the lower magnetic fields. These magnetization behaviors coincided with those of Fe/polyimide-derived carbons [9]. The humps must be caused by the difference in the freezing temperature of the spontaneous magnetization between fine clusters of metallic Fe or Fe compounds and their relatively large particles [9].

Table 2 shows VOC removal ratios of c900-CFeA*x*. A commercially available activated carbon (AC) with A_{micro} of 1300 m^2/g and VOC degradant (FE, metallic Fe fine particles, BASF) are shown for comparison, too. There is little correlation between the VOC adsorption and A_{micro} and V_{tot} calculated by nitrogen adsorption. Especially in the c*y*-CFeA0, the VOC removal abilities have little difference despite the large difference in pore development between 700 and 900 °C carbonizations. However, the VOC

Table 2 VOC removal ratio (%) of c*y*-CFeA*x*, a commercially available activated carbon (AC), and a VOC degradant (FE)

VOC	c*y*-CFeA0		c*y*-CFeA0.05		c*y*-CFeA0.15		c*y*-CFeA1.0		AC	FE
	700 °C	900 °C	700 °C	900 °C	700 °C	900 °C	700 °C	900 °C		
A	80	97	97	97	97	97	64	55	98	4
B	0	6	77	91	72	88	0	0	98	26
C	23	0	85	48	59	41	73	52	69	0
D	43	17	99	90	82	87	67	48	74	3
E	0	0	67	91	52	86	0	4	77	11
F	54	92	99	97	95	97	49	28	94	3
G	9	0	95	87	76	82	57	48	96	0
H	98	40	99	93	99	91	82	77	78	3
I	98	47	98	92	97	93	90	93	79	4
J	87	90	100	97	97	97	63	56	94	0
K	85	97	99	98	96	97	27	25	95	0
L	90	91	100	97	100	98	79	73	95	9
M	96	95	100	98	100	99	86	83	95	5

A: benzene, B: carbon tetrachloride, C: dichloromethane, D: 1,2-dichloroethane, E: 1,1,1-trichloroethane, F: 1,1,2-trichloroethane, G: 1,1-dichloroethene, H: *cis*-1,2-dichloroethene, I: *trans*-1,2-dichloroethene, J: trichloroethene, K: tetrachloroethene, L: *cis*-1,3-dichloropropene, M: *trans*-1,3-dichloropropene

adsorption may occur on the narrower pores undetectable by nitrogen adsorption, because ethene molecules, a kind of VOCs, can be preferentially adsorbed on ultramicropores with pore width of < 0.7 nm which could be estimated by CO_2 adsorption [26].

The removal ratio of carbon tetrachloride (on the row B in the table) and some alkane components (on the rows C, D, E) of c*y*-CFeA0 are low whereas these removal ratios are improved in c*y*-CFeA0.05 and c*y*-CFeA0.15. It is well known that metallic Fe behaves excellent degradations of VOC in water and in soil [27]. However, FE gives low removal ratios of all VOC in Table 2. During the test, there were few changes in Cl^- concentration accompanied by the degradation of VOC and any clear peak indicating the degradation was not detected in the chromatogram. To achieve a sufficient degradation effect by FE may require a longer test time than 4 h. At least 24 h might be required [27]. From these results, it is implied that metallic Fe in the carbons has little effect on VOC degradation except c*y*-CFeA0 and that the Na compounds such as Na_2SO_4 formed after carbonization act as the active sites particularly for the adsorption of carbon tetrachloride and alkane compounds. The developed micropores and mesopores observed in c900-CFeA*x* except c900-CFeA1.0 could facilitate the diffusion of VOC into inside such the AC surface, therefore, bringing better VOC removal abilities than commercial AC.

Conclusions

Iron alum/carboxymethylcellulose xerogels containing Na^+ ion were converted porous carbons via the carbonization over 700 °C resulted mainly from decomposition of Na_2CO_3 by-produced in the carbons. This decomposition produced mesopores as well as micropores in carbon, those volumes decreased with increasing the Na^+ ion exchange ratio in the xerogels. The carbons also had well-dispersed ferromagnetic α-iron (iron(*cI*2)) nanoparticles and increased crystallinity due to catalytic graphitization phenomenon of iron. In addition, sulphate particles such as Na_2SO_4 and numerous holes were found scattered on the carbon surface. The α-iron provided the carbons with a typical ferromagnetization and caused the carbons to be attracted to a neodymium magnet in water, even though raw CMC-derived carbon did not because of its diamagnetism. Some of the presented carbons demonstrated good VOC removal ability comparable to that of commercially available AC. This VOC adsorption increase might be due to the pore developments as well as to the chemical interaction of VOC with the by-products with Na species not but metallic Fe. Especially,

Na_2SO_4 formed after carbonization possibly acted as the active site particular for the adsorption of carbon tetrachloride and alkane compounds.

Acknowledgements

The authors thank Dr. Masanori Nagao from University of Yamanashi for the magnetization measurements and his valuable advice. FE-SEM-EDX was a shared equipment at Center for Instrument Analysis, University of Yamanashi.

Authors' contributions

NM: Conceptualization, metrology and writing original draft preparation. KH: Formal analysis and investigation. HS: Investigation and writing-review and editing. KS: Formal analysis and investigation.

Funding

This work was supported by JSPS KAKENHI Grant Numbers JP15K06438 and 19K0500.

Data Availability

The datasets generated during and/or analyzed during current study are available from the corresponding author (N.M.) on reasonable request.

Code availability

Not applicable.

Declarations

Conflict of interests The authors declare that they have no known competing financial interests or personal relationships that could have appeared to influence the work reported in this paper.

Supplementary Information: The online version contains supplementary material available at https://doi.org/10.1007/s10853-022-07578-x.

References

[1] Marchand A (1971) Electronic properties of doped carbons. In: Walker PL (ed) Chemistry and physics of carbon. Marcel Dekker Inc., New York, pp 155–191

[2] Bhatnagar A, Hogland W, Marques M, Sillanpää M (2013) An overview of the modification methods of activated carbon for its water treatment applications. Chem Eng J 219:499–511. https://doi.org/10.1016/j.cej.2012.12.038

[3] Sultana M, Sabrin RMH, M, Rahaman Md. H, Alam N. S. M, (2022) A review on experimental chemically modified activated carbon to enhance dye and heavy metals adsorption. Clean Eng Technol. https://doi.org/10.1016/j.clet.2021.100382

[4] Park JH, Hwang RH, Yoon HC, Yi KB (2019) Effects of metal loading on activated carbon on its adsorption and desorption characteristics. J Ind Eng Chem 74:199–207. https://doi.org/10.1016/j.jiec.2019.03.004

[5] Gopalan J, Buthiyappan A, Raman AAA (2022) Insight into metal-impregnated biomass based activated carbon for enhanced carbon dioxide: a review. J Ind Eng Chem. https://doi.org/10.1016/j.jiec.2022.06.026

[6] Xiao W, Jiang X, Liu X, Zhou W, Garba ZN, Lawan I, Wang L, Yuan Z (2021) Adsorption of organic dyes from wastewater by metal-doped porous carbon materials. J Clean Prod 284:124773. https://doi.org/10.1016/j.jclepro.2020.124773

[7] Dobrowolski R, Otto M (2013) Preparation and evaluation of Ni-loaded activated carbon for enrichment of arsenic for analytical and environmental purpose. Microporous Mesoporous Mater 179:1–9. https://doi.org/10.1016/j.micromeso.2013.05.017

[8] Li X, Wang H, Shao G, Wang G, Lu L (2019) Low temperature reduction of NO by activated carbons impregnated with Fe based catalysts. Int J Hydrogen Energy 44:25265–25275. https://doi.org/10.1016/j.ijhydene.2019.04.008

[9] Kaburagi Y, Hishiyama Y, Oka H, Inagaki M (2001) Growth of iron clusters and changes of magnetic properties with carbonization of aromatic polyimide film containing iron complex. Carbon 39:593–603. https://doi.org/10.1016/S0008-6223(00)00166-4

[10] Tamai H, Katsu N, Ono K, Yasuda H (2001) Antibacterial activated carbons prepared from pitch containing organometallics. Carbon 39:1963–1969. https://doi.org/10.1016/S0008-6223(01)00003-3

[11] Nakagawa H, Watanabe K, Harada Y, Miura K (1999) Control of micropore formation in the carbonized ion exchange resin by utilizing pillar effect. Carbon

37:1455–1461. https://doi.org/10.1016/S0008-6223(99)00008-1

[12] Inagaki M, Okada Y, Miura H, Konno H (1999) Preparation of carbon-coated transition metal particles from mixtures of metal oxide and polyvinylchloride. Carbon 37:329–334. https://doi.org/10.1016/S0008-6223(98)00200-0

[13] Konno H, Takahashi Y, Habazaki H (2004) Formation of iron dispersed graphite composites utilizing exfoliated graphite and their magnetic properties. Tanso 214:191–193. https://doi.org/10.7209/tanso.2004.191

[14] Bezerra CWB, Zhang L, Lee K, Liu H, Marques ALB, Marques EP, Wang H, Zhang J (2008) A review of Fe-N/C and Co-N/C catalysts for the oxygen reduction reaction. Electrochim Acta 53:4937–4951. https://doi.org/10.1016/j.electacta.2008.02.012

[15] Zhang XH, Zhang ZJ, Xie DH, Chen XY (2014) Synthesis and supercapacitor application of nanoporous carbon by the direct carbonization of aluminum salicylate coordination polymer. J Alloys Compd 607:23–31. https://doi.org/10.1016/j.jallcom.2014.04.074

[16] Wang G, Qin J, Zhao Y, Wei J (2019) Nanoporous carbon spheres derived from metal-phenolic coordination polymers for supercapacitor and biosensor. J Colloid Interface Sci 544:241–248. https://doi.org/10.1016/j.jcis.2019.03.001

[17] Yan X, Li X, Yan Z, Komarneni S (2014) Porous carbons prepared by direct carbonization of MOFs for supercapacitors. Appl Surf Sci 308:306–310. https://doi.org/10.1016/j.apsusc.2014.04.160

[18] Farid S, Ren S, Hao C (2018) MOF-derived metal/carbon materials as oxygen evolution reaction catalysts. Inorg Chem Commun 94:57–74. https://doi.org/10.1016/j.inoche.2018.06.008

[19] Ishitsuka T (1970) Sodium-carboxymethyl cellulose and its use for food processing. J Jpn Soc Food Sci Technol (Nippon Shokuhin Kagaku Kougaku Kaishi) 17:211–220. https://doi.org/10.3136/nskkk1962.17.211

[20] Yamaguchi Y, Preparation and composition of carboxymethylcellulose gels. JP patent 1984-108045

[21] Mondo M, Tamura K, Hanada N, Preparation method of hydrogel, JP patent 3389598

[22] Miyajima N, Matsumura T, Yanagisawa T, Sakane H (2021) Simultaneous control of the pore and the surface wettability in porous carbons prepared by carbonization of iodine-treated cellulose derivatives. J Porous Mater 28:271–277. https://doi.org/10.1007/s10934-020-00986-x

[23] Kaneko K, Ishi C, Ryobolt T (1994) Superhigh surface area determination of microporous carbons. In: Rouquerol J, Rodŕiguez-Reinoso F, Sing KSW, Unger KK (eds) Characterization of porous solid III in studies in surface science and catalysis. Elsevier, Amsterdam, p 583

[24] Ding L, Zhou Z, Guo Q, Huo W, Yu G (2015) Catalysis effects of Na_2CO_3 additive on coal pyrolysis and gasification. Fuel 142:134–144. https://doi.org/10.1016/j.fuel.2014.11.010

[25] Oya A, Marsh H (1982) Phenomena of catalytic graphitization. J Mater Sci 17:309–322. https://doi.org/10.1007/BF00591464

[26] Miyajima N, Hirooka K, Sakane H, Furuya M, Tamura K, Matsumoto Y (2011) Pore structures and ethylene adsorption behavior of polysaccharide-derived carbons. Tanso 249:179–184. https://doi.org/10.7209/tanso.2011.179

[27] Johnson TL, Sherer MM, Trantnyek PG (1996) Kinetics pf halogenated organic degradation by iron meatal. Environ Sci Technol 30:2634–2640. https://doi.org/10.1021/es9600901